



1 **Sources and characteristics of terrestrial carbon in Holocene-**  
2 **scale sediments of the East Siberian Sea**

3  
4 Kirsi Keskitalo<sup>1</sup>, Tommaso Tesi<sup>1,3,4</sup>, Lisa Bröder<sup>1,3</sup>, August Andersson<sup>1,3</sup>, Christof Pearce<sup>2,3</sup>,  
5 Martin Sköld<sup>5</sup>, Igor P. Semiletov<sup>6,7,8</sup>, Oleg V. Dudarev<sup>7,8</sup> and Örjan Gustafsson<sup>1,3,\*</sup>

6  
7 <sup>1</sup>Department of Environmental Science and Analytical Chemistry, Stockholm University, Stockholm, SE 10691,  
8 Sweden

9 <sup>2</sup>Department of Geological Sciences, Stockholm University, Stockholm, SE 10691, Sweden

10 <sup>3</sup>Bolin Centre for Climate Research, Stockholm University, Stockholm, SE 10691, Sweden

11 <sup>4</sup>CNR-National Research Council of Italy, ISMAR-Marine Science Institute, Bologna, IT 40129, Italy

12 <sup>5</sup>Department of Mathematics, Stockholm University, Stockholm, SE 10691, Sweden

13 <sup>6</sup>International Arctic Research Center, University Alaska Fairbanks, Fairbanks, AK 99775, USA

14 <sup>7</sup>Pacific Oceanological Institute, Russian Academy of Sciences, Vladivostok, RU 690041, Russia

15 <sup>8</sup>Tomsk National Research Polytechnical University, Tomsk, RU 634050, Russia

16

17 \*Correspondence to: Örjan Gustafsson ([orjan.gustafsson@aces.su.se](mailto:orjan.gustafsson@aces.su.se))

18

19 **Abstract.** Thawing of permafrost carbon (PF-C) due to climate warming can remobilise considerable amounts  
20 of terrestrial carbon from its long term storage to the marine environment. PF-C can be then buried in sediments  
21 or remineralised to CO<sub>2</sub> with implications for the carbon-climate feedback. Studying historical sediment records  
22 during past natural climate changes can help to understand the response of permafrost to current climate  
23 warming. In this study two sediment cores collected from the East Siberian Sea were used to study terrestrial  
24 organic carbon sources, composition and degradation during the past ~9,500 cal yrs BP. The <sup>14</sup>C-D-derived lignin  
25 and cutin products combined with  $\delta^{13}\text{C}$  suggest that there was a higher input of terrestrial organic carbon to the  
26 East Siberian Sea between ~9,500 and 8,200 cal yrs BP than in all later periods. This high input was likely  
27 caused by marine transgression and permafrost destabilisation in the early Holocene climatic optimum. Based  
28 on source apportionment modelling using dual-carbon isotope ( $\Delta^{14}\text{C}$ ,  $\delta^{13}\text{C}$ ) data, coastal erosion releasing old  
29 Pleistocene permafrost carbon was identified as a significant source of organic matter translocated to the East  
30 Siberian Sea during the Holocene.



## 31 **1 Introduction**

32 The amount of organic carbon (OC) stored in the northern circumpolar permafrost (PF) amounts to ~1300 Pg  
33 OC of which ~800 Pg OC is perennially frozen (the remaining ~500 Pg is non-permafrost, seasonally thawing  
34 active-layer permafrost or taliks) (Hugelius et al. 2014). Northern circumpolar soils thereby hold roughly half of  
35 the global soil OC pool (Tamocai et al., 2009). Modelled future climate scenarios predict continued amplified  
36 warming in the Arctic for the coming 100 years (IPCC, 2013). This will further destabilise permafrost, leading  
37 to increased delivery of terrestrial OC to the Arctic Ocean. The potential decomposition of this relict permafrost  
38 carbon (PF-C) and its subsequent release to the atmosphere as CO<sub>2</sub> or CH<sub>4</sub> constitutes a positive feedback to  
39 global warming (IPCC, 2013; Koven et al., 2011; Schuur et al., 2015; Shakhova et al., 2013, 2015, 2009; Vonk  
40 and Gustafsson, 2013). Considering the size of the Arctic PF-C pool it is important to better understand the  
41 dynamics and extent of its vulnerability to remobilisation in response to climate warming.

42 Many recent studies have focused on current carbon cycling in the Arctic land-ocean continuum  
43 (Anderson et al., 2009, 2011; Bröder et al., 2016a; Goñi et al., 2013; Goñi et al., 2010; Karlsson et al., 2015;  
44 Semiletov et al., 2016, 2011, 2012; Shakhova et al., 2010; Tesi et al., 2014, 2016b; Vonk et al., 2010;  
45 Winterfeld et al., 2015b) with possible linkages to climate change. Constraining how this system responded to  
46 earlier climate warming may help us to better predict the future response of PF-C and its climate couplings. The  
47 last glacial-interglacial transition constituted a major climate rearrangement on Earth. The increase in mean  
48 temperature coupled with sea level rise is thought to have profoundly destabilised PF-C and further released  
49 CO<sub>2</sub> to the atmosphere (Ciais et al. 2013; Crichton et al. 2016; Tesi et al. 2016a). Several studies have suggested  
50 that there was a warming-coupled translocation of terrestrial carbon during the climate warming that ended the  
51 latest glacial period (e.g., Bauch et al. 2001; Ciais et al. 2013; Mueller-Lupp et al. 2000; Tesi et al. 2016a)  
52 similar to what is predicted to happen as a consequence of the anthropogenic climate change (Barnhart et al.  
53 2014; Vonk and Gustafsson 2013).

54 Many of the previous Holocene timescale studies in the East Siberian Arctic Shelf (ESAS) have  
55 focused on the Laptev Sea (e.g., Bauch et al., 2001b; Mueller-Lupp et al., 2000; Tesi et al., 2016a). This study  
56 focuses on the East Siberian Sea (ESS) which has not yet been extensively studied in this aspect. The ESS  
57 receives terrestrial OC by coastal erosion, fluvial inflow and possibly sea bed erosion (Karlsson et al., 2016;  
58 Semiletov et al., 2005; Stein and Macdonald, 2004; Tesi et al., 2014, 2016b; Vonk et al., 2010). The coast of the  
59 ESS is dominated by carbon-rich Ice Complex Deposits (ICD) consisting of old Pleistocene material  
60 (Schirrmeister et al. 2011; Semiletov 1999a, 1999b; Vonk et al. 2012). These large ICD bluffs are vulnerable to  
61 coastal erosion (Semiletov et al., 2013; Stein and Macdonald 2004; Schirrmeister et al. 2011; Vonk et al. 2012).  
62 Coastal erosion can be further intensified with warming enhanced processes like loss of sea ice cover, increasing  
63 frequency of storms, degradation of ice-bonded coasts and sea level rise (Barnhart et al., 2014; Jones et al.,  
64 2009; Stein and Macdonald, 2004). The largest rivers directly emptying into the ESS are Indigirka and Kolyma  
65 with suspended matter discharge of  $11.1 \times 10^{12} \text{ g yr}^{-1}$  and  $123 \pm 19 \times 10^9 \text{ g yr}^{-1}$  (Gordeev, 2006; McClelland et al.,  
66 2016, respectively), with an input also from the Lena River. The Lena River drains into the Laptev Sea but its  
67 exported terrestrial OC is also transferred to the ESS via the Siberian Coastal Current (e.g., Alling et al., 2012;  
68 Sánchez-García et al., 2011). However, studies by Vonk et al. (2010, 2012) suggest that the contribution of ICD-  
69 PF erosion to the ESS sediment OC dominates over river discharge (ranging from 36 to 76 % in comparison to  
70 5–35 %, respectively). Similar observation have been made in the Laptev Sea by Semiletov et al., (2005, 2011,  
71 2012) and Vonk et al., (2012, 2014) concluding that the effect of the Lena River input is overall smaller than  
72 that from the coastal erosion.



73            In this study we investigate land-to-ocean transfer and fate of PF-C from the last post-glacial eustatic  
74 sea level rise until the present day. Our main objectives are to determine the sources and remobilisation fluxes of  
75 terrestrial OC as well as the composition and degradation status of the OC that was buried in ESS sediments  
76 during the Holocene. We characterise the OC composition by quantifying lignin phenols, cutin acids and other  
77 compounds yielded upon CuO oxidation to constrain the sources and degradation status of PF-C as well as the  
78 contribution of marine OC. Furthermore, we use a mixing model based on the isotopic composition ( $\Delta^{14}\text{C}$ ,  $\delta^{13}\text{C}$ )  
79 of the deposited OC to quantify the contribution of three different sources: topsoil-PF from active-layer  
80 deepening, ICD-PF and marine plankton. Additionally, we study how OC deposition fluxes have changed over  
81 time in response to the sea level rise and Holocene warming.



## 82 2 Materials and methods

### 83 2.1 Background and study area

84 The East Siberian Sea (ESS) is located off the northeast Siberian coast between the Laptev Sea and the Chukchi  
85 Sea (Fig. 1). The ESS is one of the largest shelf seas (987,000 km<sup>2</sup>) in the Arctic Ocean as well as one of the  
86 shallowest (mean depth 52 m) (Jakobsson, 2002).

87 Thermokarst landscapes (i.e. thawing ice-rich permafrost) cover ~20 % (3.6 x 10<sup>6</sup> km<sup>2</sup>) of the northern  
88 circumpolar permafrost region (Olefeldt et al., 2016). Ice Complex Deposit and thermokarst landscapes cover  
89 2,400 km of the ESS coastline (Grigoriev 2003). The modern average rate of coastal retreat in the ESS and the  
90 adjacent Laptev Sea is 1–10 m yr<sup>-1</sup> (Grigoriev 2010), though locally, even higher retreat rates (up to 24 and 30 m  
91 yr<sup>-1</sup>) have been reported in the most actively eroding parts (Kanevskiy et al., 2016; Romanovskii et al., 2004).  
92 The coastal erosion rates have increased in the Arctic in recent decades (Barnhart et al., 2014; Günther et al.,  
93 2015; Jones et al., 2009). According to recent studies (e.g., Bröder et al., 2016a; Semiletov et al., 2013; Tesi et  
94 al. 2016b; Vonk et al. 2012) a large fraction of the remobilised PF-C is degraded during cross-shelf transport  
95 and released back to the contemporary carbon cycle. To better predict the consequences of the permafrost thaw,  
96 it is important to understand both the amount of remobilised organic carbon as well as its fate.

97 The shelf of the East Siberian Sea contains terrestrial permafrost formed during the sea level low of last  
98 glacial maximum (Jakobsson et al. 2014). During the Pleistocene-Holocene transition the ESAS was flooded  
99 when the sea level rose rapidly (Lambeck et al., 2014; Mueller-Lupp et al., 2000). This global marine  
100 transgression started ~20,000 cal yrs BP (Lambeck et al., 2014) and flooded the ESAS between ~11,000 to  
101 ~7,000 cal yrs BP (Bauch et al. 2001a; Mueller-Lupp et al., 2000). The sampling site of the sediment core  
102 investigated in this study was flooded around 11,000 cal yrs BP (Lambeck et al., 2014). Post-glacial sea level  
103 rise with warming and wetting of the climate caused a major relocation of permafrost carbon from land to the  
104 Arctic Ocean (Bauch et al. 2001; Tesi et al. 2016a). Today the period with sea ice in the ESS is on average  
105 3 months per year which is one of the reasons why the area remains fairly unstudied (Stein and Macdonald,  
106 2004; Vetrov and Romankevich, 2004).

107

### 108 2.2 Sampling

109 A gravity core (called GC58) was collected in the East Siberian Sea at 54 m water depth as a part of the  
110 international SWERUS-C3 research expedition on i/b *Oden* in July–August 2014. The coring site (Leg 1, station  
111 58, 74.4387° N, 166.0467° E) is located ~500 km from the modern shoreline (Fig. 1). An additional sediment  
112 core was collected at the same site (MUC58) using a sediment multicorer (Oktopus GmbH, Germany), which is  
113 specifically designed to preserve the sediment-water interface. The total length of GC58 was 78 cm while  
114 MUC58 was 32 cm long. The GC58 core was split in half during the expedition and kept refrigerated (+4° C). In  
115 the laboratory at Stockholm University, one half was subsampled at 1 cm intervals and kept frozen at -18° C.  
116 The multicore was sliced during the expedition at 1 cm intervals and then immediately frozen (-18° C). Prior to  
117 analyses, the samples were freeze-dried at the Department of Environmental Science and Analytical Chemistry,  
118 Stockholm University, Sweden.

119

### 120 2.3 <sup>210</sup>Pb dating

121 Radiogenic <sup>210</sup>Pb was analysed with a gamma-ray spectrometer (GRS) at the Department of Geology of the  
122 Swedish Museum of Natural History in Stockholm, Sweden. The GRS determines the decay energy of  
123 radioisotopes in counts per second by measuring gamma emission of the sample at a known energy level.



124 Prior to the GRS analysis, a subsample of approximately 10 g was homogenised and placed in a plastic  
125 container for at least three weeks to reach secular equilibrium between the radioisotopes of lead and radium  
126 ( $^{210}\text{Pb}$  and  $^{226}\text{Ra}$ , respectively). The samples were analysed for  $^{210}\text{Pb}$  (46.51 keV),  $^{226}\text{Ra}$  (186.05 keV) and  $^{137}\text{Cs}$   
127 (661.66 keV) on an EG&G ORTEC® co-axial low energy photon spectrometer containing a High-Purity  
128 Germanium detector. The counting period for each sample lasted from 1–3 days depending on the amount of  
129  $^{210}\text{Pb}$  in the sample. An externally calibrated U-series standard (pitchblende, Stackebo, Sweden) was used to  
130 determine the relative efficiency of the gamma detector system. For each sample a minimum of 350 counts was  
131 acquired. A blank (empty container) sample was measured to correct for the background activity. The original  
132 method is described in detail by Elmquist et al., (2007).

133 Two different models were used for the  $^{210}\text{Pb}$  dating: CRS (constant rate of supply) model which  
134 assumes a constant rate of supply of excess  $^{210}\text{Pb}$  fallout, and CIC (constant initial concentration) model which  
135 assumes constant initial concentration of excess  $^{210}\text{Pb}$  (Appleby and Oldfield, 1977).

136

#### 137 **2.4 Bayesian modelling of $^{14}\text{C}$ ages for the chronology**

138 For the age-depth model construction, molluscs retrieved from GC58 were analysed for their radiocarbon ( $^{14}\text{C}$ )  
139 content at the US-NSF National Ocean Sciences Accelerator Mass Spectrometry (NOSAMS) Facility at the  
140 Woods Hole Oceanographic Institution (WHOI), MA, USA. The analysis followed their standard procedures  
141 (Pearson et al., 1998) (Table 1).

142 To account for natural differences in the amount of  $^{14}\text{C}$  in the atmosphere as well as differences  
143 between the marine environment and the atmosphere (e.g., Stuiver and Braziunas 1993), all  $^{14}\text{C}$  data were  
144 calibrated with the Marine13 calibration curve. The offset in the local reservoir age was taken into account by  
145 using a  $\Delta R$  of  $50 \pm 100$  years. Since there are no  $\Delta R$  values for the ESS in the literature, this  $\Delta R$  value was taken  
146 from a study in the Laptev Sea (Bauch et al. 2001a). The radiocarbon dates are reported in conventional  
147 radiocarbon ages (cal yrs BP) (Stuiver and Polach 1977).

148 The age model of the core was built with the OxCal v4.2 program based on the radiocarbon dated  
149 molluscs and a depositional model (P\_sequence,  $k = 0.5$ ) (Bronk Ramsey 2008; Bronk Ramsey and Lee 2013).  
150 Also, the base of the adjacent multicore dated with  $^{210}\text{Pb}$  was used in the model. The  $^{210}\text{Pb}$  date used was an  
151 average age (50 yrs BP) from the two  $^{210}\text{Pb}$  dating models (CRS, CIC) for the bottom layer (12.5 cm) of the  
152 multicore (Supplementary Table S3). The age model of GC58 was constructed with a Bayesian statistics  
153 approach using the reservoir age ( $\Delta R$ ) and the depth as a prior model and measured radiocarbon dates as  
154 likelihoods. The posterior probability densities were acquired with a Markov Chain Monte Carlo procedure  
155 which calculates possible distributions in order to date each sediment layer using the given prior model and  
156 likelihoods (Bronk Ramsey 2008).

157 Sampling with a heavy gravity corer often disturbs the sediment-water interface and thereby causes  
158 losses of the surface sediments. The organic carbon (OC) content of GC58 was therefore compared to the OC  
159 content of the adjacent MUC58 to identify for the possible loss. According to the comparison, the top 3 cm were  
160 likely lost in GC58 (Supplementary Fig. S1), and thus corrected for.



## 161 2.5 Alkaline CuO oxidation

162 Microwave assisted alkaline CuO oxidation was carried out using the method by Goñi and Montgomery (2000).  
163 Each homogenised subsample of around 300 mg was mixed with 300 mg of cupric oxide (CuO) and 50 mg of  
164 ammonium iron (II) sulphate hexahydrate ((NH<sub>4</sub>)<sub>2</sub>Fe(SO<sub>4</sub>)<sub>2</sub>·6H<sub>2</sub>O). After thorough mixing, nitrogen-purged 2M  
165 NaOH was added to each sample. Alkaline oxidation was performed with an UltraWAVE Milestone 215  
166 microwave digestion system at 150°C for 90 min.

167 A known amount of internal recovery standards (ethyl-vanillin, cinnamic acid) was added to the CuO  
168 reaction products and then acidified to pH 1 with concentrated HCl (35 %). The CuO reaction products were  
169 repeatedly extracted using ethyl acetate (EtOAc). Anhydrous sodium sulphate (NaSO<sub>4</sub>) was added to remove the  
170 remaining water. The extracts were dried in a CentriVap (Christ RVC 2-25) at 60° C, re-dissolved in pyridine  
171 and stored in a freezer (-18° C) until further analysis.

172 Finally, the samples were analysed with a gas chromatograph mass spectrometer (GC-MS, Agilent  
173 7820A) using a DB5-MS capillary column (60 m x 250 µm, 0.25 µm stationary phase thickness, Agilent J&W)  
174 at an initial temperature of 60° C, followed by a ramp of 5° C/min until reaching 300° C. Prior to the GC-MS  
175 analysis, the extracts were derivatised with *bis*-trimehtylsilyl trifluoroacetamide (BSTFA) + 1 %  
176 trimethylchlorosilane (TMCS) to silylate exchangeable hydrogens. The quantification of the samples was based  
177 on the comparison of the key ions to commercially available standards. Concentrations of CuO oxidation  
178 products were normalised to the organic carbon content of the sample and are reported as mg g<sup>-1</sup> OC.

179

## 180 2.6 Bulk organic carbon and stable carbon isotope analyses

181 For the total organic carbon content (TOC), the total nitrogen content (TN) and the stable carbon isotope  
182 analysis (δ<sup>13</sup>C) of TOC, subsamples of 10–15 mg were homogenised and placed in silver capsules, acidified  
183 with 1.5M HCl to remove carbonates and then dried at 60° C. The TOC, TN and δ<sup>13</sup>C-TOC were quantified with  
184 an elemental analyser Carlo Erba NC2500 connected via a split interface to a Finnigan MAT Delta V mass  
185 spectrometer at the Stable Isotope Laboratory of the Department of Geological Sciences at Stockholm  
186 University.

187 For radiocarbon (<sup>14</sup>C) analysis of the bulk organic carbon, subsamples of sediment were acidified with  
188 1.5M HCl and sent to NOSAMS. To account for the time between the deposition and the measurement, the <sup>14</sup>C  
189 dates were calibrated with the Eq. (1) using the age data derived from the age model. The bulk radiocarbon data  
190 are reported as Δ<sup>14</sup>C (Stuiver and Polach 1977).

191

$$192 \Delta^{14}\text{C} = (\text{Fm} \times e^{\lambda(1950-Y_c)} - 1) \times 1000 \quad (1)$$

193

194 where Fm is the Fraction Modern, λ is 1/mean life of radiocarbon= 1/8267 and Y<sub>c</sub> is the year of collection  
195 derived from the age model (Stuiver and Polach, 1977).

196

## 197 2.7 Source apportionment

198 The carbon isotope fingerprint of OC (Δ<sup>14</sup>C, δ<sup>13</sup>C) can be used to quantitatively diagnose the relative  
199 contribution of topsoil-PF, ICD-PF and marine OC assuming isotopic mass balance (e.g., Vonk et al., 2012). In  
200 other words, the carbon isotopic signatures may help to understand whether the OC comes from coastal erosion  
201 as a result of the post-glacial warming and sea level rise, active-layer deepening of permafrost carbon in the  
202 watershed (as a response to the post-glacial warming) or sedimentation of marine phytoplankton. These different



203 sources have a natural variability in their isotopic composition (end-members). This variability needs to be taken  
204 into account to correctly estimate the relative source contributions and the associated uncertainties (e.g.,  
205 Andersson, 2011). In previous studies a Bayesian Markov Chain Monte Carlo (MCMC) driven approach has  
206 been used to effectively estimate the relative source contributions for individual data points (Andersson et al.,  
207 2015; Tesi et al., 2016a). Here, we expand this approach to include the time-dependence of the down-core  
208 isotopic signatures, taking an advantage of the relatively small variability of the 78  $\delta^{13}\text{C}$  data points, whilst also  
209 using the 10  $\Delta^{14}\text{C}$  points. The time-dependence of different proportions was taken into account by following the  
210 approach of Parnell et al. (2012). The method is described in detail in the Supplementary Methods.

211 The end-member values for the three source classes were taken from the literature (Bröder et al.,  
212 2016b; Tesi et al., 2016a) topsoil-PF ( $\Delta^{14}\text{C}=-232\pm 147$  ‰,  $\delta^{13}\text{C}=-26.95\pm 1.17$  ‰; mean  $\pm$  standard deviation),  
213 representing thaw of the active-layer of permafrost; marine OC ( $\Delta^{14}\text{C}=-50\pm 12$  ‰,  $\delta^{13}\text{C}=-20.97\pm 2.56$  ‰),  
214 resulting from primary production of phytoplankton; and ICD-PF ( $\Delta^{14}\text{C}=-940\pm 31$  ‰,  $\delta^{13}\text{C}=-26.3\pm 0.63$  ‰),  
215 resembling the old Pleistocene material from coastal erosion. The end-member value for ICD-PF was corrected  
216 with Eq. (1) to account for the age of the deposition.

217

## 218 2.8 Grain size analysis

219 Prior to the grain size analysis subsamples of sieved (500  $\mu\text{m}$ ) sediments from GC58 were homogenised. The  
220 grain size analysis was done with a Malvern Mastersizer 3000 laser diffraction particle size analyser, which can  
221 measure particles between 10 nm and 3.5 mm. Sodium hexametaphosphate (10 %) was used to disaggregate the  
222 particles suspended in deionised water. To further aid the disaggregation, all samples were exposed to  
223 ultrasound for 60 s and allowed to disperse in continuous flow for 3 min in total (including 60 s of  
224 ultrasonication) prior to the measurements. To control the concentration of the sample in the flow during the  
225 measurements, the obscuration was kept between 5–15 %. High sample obscuration (i.e. high concentration) would  
226 cause multiple light scatterings, thus distorting the results. Each sample was analysed in five replicates. The  
227 measurements were carried out at the Department of Geological Sciences at Stockholm University, Sweden.



## 228 **3 Results and Discussion**

### 229 **3.1 Age chronology of the core**

230 The deepest part of the sediment core GC58 dates back ~9,500 cal yrs BP i.e. to the early Holocene. The age-  
231 depth model shows an evident hiatus in the middle of the core between 39.5 cm and 40.5 cm resulting in an age  
232 gap of ~6,500 years (~8,200–1,700 cal yrs BP) (Fig. 2). In addition, there is a shorter gap in the chronology  
233 between ~9,300 and ~8,500 cal yrs BP. In studies from the adjacent Laptev Sea such age discrepancies have not  
234 been observed (Bauch et al. 2001a; Bauch et al. 2001b; Tesi et al. 2016a). It therefore seems likely that there has  
235 been a local event causing the removal of sediment layers. There might not have been accumulation during  
236 those periods, or the age gap could be a condensed unit of sediment. Although any actual sediment transport  
237 processes giving rise to such a putative total halt in the sedimentation rate is rather elusive and unlikely. Since  
238 the whole East Siberian Arctic Shelf (ESAS) is a very shallow shelf where sea ice is formed (Conlan et al.,  
239 1998; Jakobsson, 2002), a likely explanation for an age gap is ice scouring as observed in the Laptev Sea  
240 (Ananyev et al., 2016). An ice scouring event could have formed a gouge at the sea bottom that later was re-  
241 filled with sediment (Barnes et al. 1984).

242 The accumulation rates of GC58 obtained from the  $^{14}\text{C}$  measurements vary between 0.2 and 1.4 mm yr $^{-1}$   
243 (17.0–138.9 cm kyr $^{-1}$ ) and mass accumulation rates (MAR) spanned 0.02–0.1 g cm $^{-2}$  yr $^{-1}$ . Bauch et al. (2001a)  
244 have reported similar sedimentation rates (0.1–2.6 mm yr $^{-1}$ ) from the outer shelf of the Laptev Sea around the  
245 same time period. The linear sedimentation rate for the adjacent sediment core MUC58 derived from  $^{210}\text{Pb}$   
246 dating is 1.3 mm yr $^{-1}$  and an average MAR 0.03 g cm $^{-2}$  yr $^{-1}$ . Similar accumulation rates with  $^{210}\text{Pb}$  dated sediment  
247 cores have been reported in other studies from the East Siberian Sea: 1.1–1.6 mm yr $^{-1}$  (Vonk et al. 2012) and  
248 1.4–1.5 mm yr $^{-1}$  (Bröder et al., 2016b). The slight difference in accumulation rates using  $^{210}\text{Pb}$  chronology  
249 compared to  $^{14}\text{C}$  may be due to active biological mixing giving higher accumulation rates for the shorter time  
250 scale of more surficial sediments (Baskaran et al. 2016; Boudreau 1994).

251

### 252 **3.2 Sediment grain size, stable carbon isotopes and biomarker composition of organic matter**

253 Grain size can be used to describe the depositional environment. The sediment core GC58 consists mostly of  
254 clay and silt, with a fraction of sand (Supplementary Fig. S2). The higher sand content that is observed at ~8,500  
255 cal yrs BP may reflect a higher-energy depositional regime likely due to proceeding marine transgression and  
256 energetic coastal dynamics. Bauch et al. (2001a) have reported a shift from sandy silt to clayey silt around 7,400  
257 cal yrs BP from a sediment core collected in the eastern Laptev Sea. They attribute this change to the end of the  
258 sea level rise and the establishing of more stable conditions. The GC58 sediment core has a hiatus at that time  
259 period but has a similar clayey silt composition at the top part of the core (~1,700 cal yrs BP until today). This  
260 may indicate comparably similar stable conditions in the East Siberian Sea in the last 1,700 cal yrs BP.

261 The total organic carbon (TOC) concentrations in GC58 vary from 0.5 to 1.1% (Supplementary Table  
262 S1) with the highest TOC content in the surface sediments. These data agree with average TOC contents  
263 reported for the East Siberian Sea (Semiletov et al., 2005; Stein and Macdonald, 2004; Vetrov and  
264 Romankevich, 2004; Vonk et al., 2012). The OC fluxes for GC58 calculated with the  $^{14}\text{C}$  age-model (covering  
265 ~9,500 cal yrs BP) range between 1.2 and 10.9 g m $^{-2}$  yr $^{-1}$  (Fig. 3a). The OC fluxes for MUC58 calculated with  
266 the  $^{210}\text{Pb}$  chronology (covering the most recent ~100 yrs) are similar and vary from 0.4 to 6.1 g m $^{-2}$  yr $^{-1}$   
267 (Supplementary Table S2). The OC fluxes show an increasing trend from the bottom of the core toward the top  
268 in both cores. A similar trend has been reported by (Bröder et al., 2016b) from the East Siberian Sea using two  
269  $^{210}\text{Pb}$ -dated sediment cores. For GC58, the high OC flux at the very top of the core is likely related to the





270 merging of the two dating systems ( $^{14}\text{C}$  and  $^{210}\text{Pb}$ ), which causes a higher sediment accumulation rate at the top  
271 of the core and thus higher fluxes.

272 Lignin phenols and cutin acids are useful proxies for tracing carbon of terrestrial origin because both  
273 compounds are solely biosynthesised in terrestrial plants. Lignin is an essential component in cell walls of  
274 vascular plants (Higuchi, 1971), while cutin is a lipid polyester, which forms a protective wax layer on  
275 epidermal cells of leaves and needles with other lipids (e.g., Kunst and Samuels 2003). These compounds have  
276 been widely used in recent studies of terrestrial OC in the Arctic (e.g., Amon et al., 2012; Bröder et al., 2016b;  
277 Goñi et al., 2013; Tesi et al., 2014). Both lignin and cutin fluxes show a similar trend with the highest fluxes at  
278 the bottom of the core (~9,500 cal yrs BP) indicating a high proportion of terrestrial organic matter (Fig. 3b).  
279 The large variability in the fluxes between ~9,500 and ~8,200 cal yrs BP compared to the latest ~1,700 cal yrs  
280 BP suggests that the system was more dynamic at that time. The rapid decrease in both lignin and cutin fluxes  
281 proposes a change from terrestrially dominated to marine dominated input at ~8,400 cal yrs BP in this part of  
282 the East Siberian Sea. Bauch et al. (2001b) suggested a similar regime shift from terrestrial to marine in the  
283 Laptev Sea between ~8,900 and ~8,400 cal yrs BP based on the occurrence of bivalves and benthic  
284 foraminiferal species. The same process affecting OC fluxes is likely causing also higher lignin and cutin fluxes  
285 at the top of GC58. The overall decrease in lignin and cutin fluxes as well as concentrations (Supplementary  
286 Table S3) in time is likely due to increasing hydrodynamic sorting and degradation during transport as transport  
287 times from the coast became longer because of the marine transgression (Fig. 3a). Bröder et al., (2016a) have  
288 observed a similar strong decrease in the amount of terrestrial organic carbon depositions with increasing  
289 distance from the coast in the Laptev Sea. A recent study by Tesi et al. (2016b) shows that the largest particles,  
290 rich in lignin (i.e. plant debris), tend to be preferentially buried close to the shore and with cross-shelf transport  
291 of lignin occurring overwhelmingly bound to fine particles (with low settling velocities) (i.e. of the total lignin  
292 deposited to the marine environment only a fraction, ~4–5 %, travels across the shelf).

293 Other useful indicators of the marine input in organic matter are CuO oxidation derived low-molecular  
294 weight fatty acids (LMW-FA). They are mainly found in phytoplankton but also in other organisms such as  
295 bacteria and algae (Goñi and Hedges, 1995). Especially C16FA:1 together with C14FA and C16FA serve as  
296 proxies for marine OC as they are highly abundant in marine sediments and very low in concentrations in ICD-  
297 PF and topsoil-PF (Goñi and Hedges, 1995; Tesi et al., 2014). The highest fluxes of LMW-FA are observed for  
298 the very top of the core (Fig. 3c), indicating a larger proportion of marine OC. The values decrease rapidly  
299 down-core as marine FA are readily degraded (e.g., Bröder et al., 2016b; Canuel and Martens, 1996). This trend  
300 may also be influenced by the change in input from terrestrial to marine dominated sources.

301 The stable isotopic composition of bulk OC ( $\delta^{13}\text{C}$ ) may be used to distinguish between marine and  
302 terrestrial organic matter (Fry and Sherr, 1984). The  $\delta^{13}\text{C}$  values for C3-photosynthesised terrestrial carbon are  
303 between -23 to -30 ‰, whereas marine carbon has a less depleted  $\delta^{13}\text{C}$  signature between -18 ‰ and 24 ‰ (e.g.,  
304 Fry and Sherr, 1984). However, these end-member values may differ depending on the region, especially in the  
305 Arctic where open water and sea ice phytoplankton exhibits different isotopic fingerprints (Kohlbach et al.,  
306 2016). The  $\delta^{13}\text{C}$  values for GC58 range from -23 to -25 ‰ (Fig. 3d) with the most depleted values (i.e. most  
307 terrestrial) between ~9,500 and ~8,200 cal yrs BP, and the least depleted values (i.e. most marine) from ~1,700  
308 cal yrs BP until the modern time. Mueller-Lupp et al. (2000 and references within) have argued that  $\delta^{13}\text{C}$  values  
309 in sediments of the Arctic Ocean can have a terrestrial overprint in  $\delta^{13}\text{C}$  composition caused by the rapid  
310 degradation of planktonic organic matter i.e. the amount of marine organic matter of the total organic matter



311 pool in the Arctic is relatively low. Yet, the gradual change in  $\delta^{13}\text{C}$  indicates that the contribution of marine  
312 organic matter is greater at the top of the core where the  $\delta^{13}\text{C}$  values are less depleted.

313 It is notable that the values for all the different parameters shown in Fig. 3 on both sides of the age gap  
314 (between ~8,200 and ~1,700 cal yrs BP) are near-continuous in spite of the ~6,500 year hiatus (except for the  
315 bulk  $\Delta^{14}\text{C}$  OC values). This could be explained by bioturbation, mixing the older part of the core with the newer  
316 deposits, thus resulting in an apparent continuity in property values across the hiatus. The  $\Delta^{14}\text{C}$  values suggest  
317 that there was more  $^{14}\text{C}$  depleted material deposited ~1,600 cal yrs BP ago, causing a drop in the  $\Delta^{14}\text{C}$  values.  
318 Though more likely, as the  $\Delta^{14}\text{C}$  values are dependent on time, any uncertainty in the age model would have an  
319 effect on the  $\Delta^{14}\text{C}$  values.

320

### 321 3.3 Degradation status of terrestrial organic matter

322 Lignin phenols provide insight to the degradation status of the deposited terrestrial organic matter. The acid-to-  
323 aldehyde ratios of lignin phenols, syringic acid to syringaldehyde (Sd/SI) and vanillic acid to vanillin (Vd/VI),  
324 have been used to study degradation of lignin (e.g., Benner and Opsahl, 1995; Hedges et al., 1988). As acids are  
325 more abundant in relation to aldehydes in degraded lignin, higher ratios mean more degraded lignin (Goñi et al.,  
326 1993). Both Sd/SI and Vd/VI ratios show great variability throughout the core (Fig. 4a), especially for the top  
327 part of the core. The variability at the core top may reflect the analytical uncertainty caused by very low lignin  
328 concentrations. In addition, Goñi et al. (2000) and Tesi et al. (2014) have argued that the acid to aldehyde ratios  
329 of lignin phenols might not serve as good degradation proxy for Arctic Ocean sediments as the material entering  
330 the marine environment might have experienced degradation prior to entering the marine system.

331 The ratio of 3,5-dihydrobenzoic acid to vanillyl phenols (3,5-Bd/V) is another proxy used to constrain the  
332 degradation status of terrestrial organic matter in sediments (e.g., Hedges et al. 1988; Tesi et al. 2014; Tesi et al.  
333 2016a). Specifically, this proxy is used to distinguish diagenetically-altered mineral soil OC from relatively  
334 fresh vascular plant debris (Farella et al. 2001; Louchouart et al. 1999; Prahl et al. 1994). The only source of  
335 3,5-Bd in the marine environment is from brown algae which are not common in the study area (Goñi and  
336 Hedges, 1995; Tesi et al., 2014). The low 3,5-Bd/V ratio at the bottom of the core (~9,500– 8,200 cal yrs BP)  
337 implies that the organic matter that was deposited in that period was relatively undegraded (Fig. 4b). The extent  
338 of degradation gradually increases toward the top of the core. However, hydrodynamic sorting may affect the  
339 degradation values as the largest particles of fresh vascular plant debris are likely buried close to the coast (Tesi  
340 et al., 2016b). The input of organic matter was higher before ~8,200 cal yrs BP, presumably due to coastal  
341 erosion caused by the marine transgression. When sediments are quickly buried they can serve as a more  
342 effective sink for terrestrial organic matter (Hilton et al., 2015). As the material is less degraded and the  
343 sedimentation rates are high in GC58 between ~9,500 and ~8,200 cal yrs BP, the input of organic matter was  
344 likely high causing it to be quickly buried. Similar high input of terrestrial material has been observed in the  
345 Laptev Sea ~11,000 cal yrs BP (Tesi et al. 2016a).

346 The location of the study site is currently ~500 km offshore so transport time and thereby the oxygen  
347 exposure time of the organic matter in the benthic compartment is now longer than in the earlier phase of the  
348 Holocene. The longer distance from the coast allows more time for organic matter to degrade before burial  
349 (Bröder et al., 2016a). Hartnett et al. (1998) have also shown that the burial efficiency of organic carbon  
350 decreases as a function of oxygen exposure time. The same trend can be seen in the fraction remaining lignin  
351 ( $f_{\text{lignin/terrOC}}$ ) i.e. the amount of lignin as a ratio of the observed and expected (assuming conservative mixing i.e.  
352 no degradation) concentrations of lignin and terrestrial OC (terrOC) (see Supplementary Methods for details). In



353 GC58 the  $f_{\text{lignin/terrOC}}$  decreases down-core likely as a result of the proceeding marine transgression  
354 (Supplementary Fig. S3). This trend suggests that with longer transport time the lignin degradation is more  
355 extensive due to the protracted oxygen exposure time and hydrodynamic sorting (Keil et al., 2004; Tesi et al.,  
356 2016a). We estimated this lateral transport time to be  $\sim 1.4$  kyr longer at modern times than at the beginning of  
357 the Holocene for the station GC58 (Supplementary Fig. S4). To model the lateral transport times, we used the  
358  $f_{\text{lignin/terrOC}}$  with individual degradation rates for terrOC and lignin (Bröder et al. 2017, submitted) (see  
359 Supplementary Methods).

360

### 361 3.4 Dual-isotope based source apportionment of OC

362 The source apportionment results show that most of the organic matter originates from coastal erosion since  
363 ICD-PF material is the largest fraction (41–91 %) throughout the core (Fig. 5). Earlier studies demonstrated that  
364 the decay of fresh marine organic matter is more rapid compared to degradation of terrestrial organic matter  
365 (Karlsson et al., 2011, 2015; Salvadó et al., 2016; Vonk et al., 2010). This may lead to selective preservation of  
366 terrestrial organic matter in the sediments of the East Siberian Arctic Shelf (Karlsson et al. 2011, 2015; Vonk et  
367 al. 2010). The proportion of old terrestrial organic matter might also be greater in Arctic sediments due to  
368 generally low primary production in the area (Stein and Macdonald, 2004). The contribution of topsoil-PF is  
369 fairly low throughout the core (3–23 %). This may be due to the location of GC58 between the two major rivers  
370 (Kolyma and Indigirka) resulting in relatively low amounts of fluvial inflow depositing topsoil permafrost.

371 To further interpret our results within a larger context of PF-C destabilisation during post-glacial  
372 warming, we compared our results with another transgressive deposit collected in the Laptev Sea (PC23, Fig. 1,  
373 Tesi et al. 2016a). For the Laptev Sea (PC23), there was a predominant influence of watershed-sourced material  
374 via river discharge during the onset of the Holocene, followed by a similar contributions of marine OC and ICD-  
375 PF fractions (both sources varying between 31 and 56 %) from  $\sim 8,300$  cal yrs BP to present. For the East  
376 Siberian Sea (GC58), the contribution of ICD-PF is more prominent for the same time period, indicating a  
377 higher significance of coastal erosion for the East Siberian Sea compared to the Laptev Sea (Fig. 6), especially  
378 when compared to the early Holocene signature. Topsoil-PF fractions in PC23 are slightly higher (8–25 %) than  
379 in GC58 (3–23 %) from  $\sim 8,300$  cal yrs BP to current day. The difference is likely caused by a strong influence  
380 of the Lena River at the sampling location of PC23 and less fluvial inflow to GC58 due to location farther away  
381 from the mouths of the Lena, Kolyma and Indigirka rivers.

382 When the shoreline was farther seaward during the early Holocene, the core PC23 from the Laptev Sea  
383 experienced a large influence of Lena River derived material (80–90 %) (Tesi et al. 2016a). This material was  
384 supplied to the Laptev Sea in response to the deglaciation and associated active-layer deepening in the  
385 watershed (Tesi et al. 2016a). Although the record of GC58 does not go back in time to the glacial-interglacial  
386 transition at the very onset of the Holocene, our results suggest that coastal erosion was likely the dominant  
387 process affecting the permafrost carbon supply and deposition also at that time. This seems likely, especially  
388 when considering the location of the core GC58 in between the rivers, and as has been observed in modern day  
389 shallower sediments in the East Siberian Sea (Bröder et al., 2016b; Vonk et al., 2012).

390



391 **3.5 Biomarker indications of sources of terrestrial organic matter**

392 The lignin fingerprint of organic matter sources in GC58 is consistent with the dual-carbon isotope modelling.  
393 Here we focus on the cinnamyl to vanillyl phenols and syringyl to vanillyl phenols ratios ( $C/V$  and  $S/V$ ,  
394 respectively). The  $C/V$  ratio can be used to differentiate between woody (i.e. shrubs and trees) and non-woody  
395 (i.e. leaves, needles, grasses) plant tissues as origin of the terrestrial OC since cinnamyl phenols are produced  
396 only in non-woody vascular plant tissues (Hedges et al., 1988). Moreover, the  $S/V$  ratio differentiates between  
397 gymnosperms (conifers) and angiosperms (flowering plants) as syringyl phenols are produced solely in  
398 angiosperms (Hedges et al., 1988). Thereby higher  $S/V$  ratios mean more contribution from angiosperm plants.

399 The  $S/V$  and  $C/V$  ratios in GC58 show that the terrestrial material transported to the ESS originates  
400 mainly from soft tissue material (i.e. grasses and leaves) both from angiosperm and gymnosperm plants (Fig. 7).

401 The lignin fingerprint of old Pleistocene material (ICD-PF) is characterised by high ratios of both  $C/V$  and  $S/V$   
402 i.e. a high abundance of soft plant tissues from the tundra steppe vegetation (e.g. grass-like material) (Tesi et al.  
403 2014; Winterfeld et al. 2015). Observations from the Laptev Sea (sediment core PC23, Fig. 1) reveal a much  
404 stronger influence from woody material indicating a watershed source, likely from the Lena River, rather than  
405 from coastal erosion (Fig. 7). It should be noted that the lignin phenols are susceptible to degradation. Cinnamyl  
406 phenols in particular are known to degrade fairly fast, which may lower the  $C/V$  ratios (Benner and Opsahl,  
407 1995). However, even considering degradation effects, the relatively high  $C/V$  and  $S/V$  values that characterise  
408 GC58, indicate grass-type material typical of tundra/steppe biome and ICD-PF deposits (Tesi et al., 2014;  
409 Winterfeld et al., 2015a).



410 **4 Conclusions**

411 This down-core study provides new insights into terrestrial carbon dynamics in the East Siberian Sea (ESS)  
412 from the early Holocene warming period until the present. Our results suggest a high input of terrestrial organic  
413 carbon to the ESS during the last glacial-interglacial period caused by permafrost destabilisation. This material  
414 was mainly characterised as relict Pleistocene permafrost deposited via coastal erosion as a result of the sea  
415 level ingression.

416 The flux rates of both lignin and cutin compounds show a declining trend from the early Holocene until  
417 today, suggesting a change from mainly terrestrial to marine dominated input. The same change can be seen in  
418 the stable carbon isotope ( $\delta^{13}\text{C}$ ) data, which imply a regime shift from terrestrial to more marine dominated  
419 sediment input at  $\sim 8,400$  cal yrs BP.

420 The source apportionment data highlights the importance of coastal erosion as a terrestrial carbon  
421 source to this region of the ESS throughout the Holocene. This is supported by the lignin composition, which  
422 suggests that the terrestrial carbon in the sediment core GC58 consists mainly of soft tissues of plants (i.e.  
423 grasses), typical for tundra/steppe vegetation during the Pleistocene. Both the biomarker and grain size data  
424 imply that the conditions have been more stable in the ESS in the past  $\sim 1,700$  cal yrs BP compared to the early  
425 Holocene.

426 The comparison of the source apportionment results ( $\delta^{13}\text{C}$ ,  $\Delta^{14}\text{C}$ ) and the lignin fingerprint (C/V and  
427 S/V ratios) for the sediment cores GC58 and PC23 show a difference in the carbon sources between the East  
428 Siberian Sea and the adjacent Laptev Sea. The relict Pleistocene permafrost, mostly originating from coastal  
429 erosion, may be more dominant in the ESS than in the Laptev Sea. Data for the sediment core PC23 show that  
430 the Laptev Sea instead had a relatively high input of terrestrial carbon from the watershed, which is likely due to  
431 the influence of the Lena River.

432 The accelerating coastal erosion rates along the Siberian coast and amplified warming in the Arctic  
433 predicted by many climate models are likely to cause permafrost destabilisation and remobilisation of terrestrial  
434 carbon to the marine environment, as observed in the beginning of the Holocene. To better understand the  
435 consequences of the permafrost thawing processes, the extent of degradation of terrestrial carbon in the marine  
436 environment should be better constrained. Also, to improve the understanding of the processes in the ESS and in  
437 the whole Arctic region more historical down-core studies would be needed.

438



439 **Author contributions**

440 T. Tesi and Ö. Gustafsson conceived and designed the research project. T. Tesi, L. Bröder, I. Semiletov, O.  
441 Dudarev and Ö. Gustafsson collected the samples with the help from the IB/RV *Oden* crew. C. Pearce and K.  
442 Keskitalo developed the age-depth model of GC58. K. Keskitalo carried out all chemical and geological  
443 analyses on GC58 and MUC58. M. Sköld and A. Andersson ran the MCMC simulation for the OC source  
444 apportionment. A. Andersson estimated the lateral transport times. K. Keskitalo wrote the paper and produced  
445 the figures with input from all the co-authors.

446

447 **Competing interests**

448 The authors declare that they have no conflict of interest.



449 **Acknowledgments**

450 We thank the crew and personnel of IB/RV *Oden*. We thank Rienk Smittenberg for the use of the microwave  
451 extraction facilities. We also thank Carina Jakobsson, Heike Siegmund and Karin Wallner for their help with the  
452 laboratory analyses. This study was supported by the Knut and Alice Wallenberg Foundation (KAW contract  
453 2011.0027), the Swedish Research Council (VR contract 621-2004-4039 and 621-2007-4631), the Nordic  
454 Council of Ministers Cryosphere-Climate-Carbon Initiative (project Defrost, contract 23001) and the European  
455 Research Council (ERC-AdG project CC-TOP #695331). Additionally, I. Semiletov thanks the Russian  
456 Government for financial support (mega-grant under contract #14.Z50.31.0012). O. Dudarev thanks the Russian  
457 Science Foundation for financial support (No. 15-17-20032). T. Tesi acknowledges EU financial support as a  
458 Marie Curie fellow (contract no. PIEF-GA-2011-300259). Contribution no. 1916 of ISMAR-CNR Sede di  
459 Bologna. L. Bröder acknowledges financial support from the Climate Research School of the Bolin Centre for  
460 Climate Research. C. Pearce received funding from the Danish Council for Independent Research / Natural  
461 Science (project DFF-4002-00098/FNU). M. Sköld acknowledges financial support from the Swedish Research  
462 Council (Grant 2013:05204).

463 **References**

- 464 Alling, V., Porcelli, D., Mörth, C. M., Anderson, L. G., Sanchez-Garcia, L., Gustafsson, Ö., Andersson, P. S.  
 465 and Humborg, C.: Degradation of terrestrial organic carbon, primary production and out-gassing of CO<sub>2</sub> in the  
 466 Laptev and East Siberian Seas as inferred from  $\delta^{13}C$  values of DIC, *Geochim. Cosmochim. Acta*, 95, 143–159,  
 467 doi:10.1016/j.gca.2012.07.028, 2012.
- 468 Amon, R. M. W., Rinehart, A. J., Duan, S., Louchouart, P., Prokushkin, A., Guggenberger, G., Bauch, D.,  
 469 Stedmon, C., Raymond, P. A., Holmes, R. M., McClelland, J. W., Peterson, B. J., Walker, S. A. and Zhulidov,  
 470 A. V.: Dissolved organic matter sources in large Arctic rivers, *Geochim. Cosmochim. Acta*, 94, 217–237,  
 471 doi:10.1016/j.gca.2012.07.015, 2012.
- 472 Ananyev, R., Dmitrevskiy, N., Jakobsson, M., Lobkovsky, L. and Nikiforov, S.: Sea-ice ploughmarks in the  
 473 eastern Laptev Sea, East Siberian Arctic shelf, , 301–302, 2016.
- 474 Anderson, L. G., Jutterström, S., Hjalmarsson, S., Wählström, I. and Semiletov, I. P.: Out-gassing of CO<sub>2</sub> from  
 475 Siberian Shelf seas by terrestrial organic matter decomposition, *Geophys. Res. Lett.*, 36(20),  
 476 doi:10.1029/2009GL040046, 2009.
- 477 Anderson, L. G., Björk, G., Jutterström, S., Pipko, I., Shakhova, N., Semiletov, I. and Wählström, I.: East  
 478 Siberian Sea, an Arctic region of very high biogeochemical activity, *Biogeosciences*, 8(6), 1745–1754,  
 479 doi:10.5194/bg-8-1745-2011, 2011.
- 480 Andersson, A.: A systematic examination of a random sampling strategy for source apportionment calculations,  
 481 *Sci. Total Environ.*, 412–413, 232–238, doi:10.1016/j.scitotenv.2011.10.031, 2011.
- 482 Andersson, A., Deng, J., Du, K., Zheng, M., Yan, C., Sköld, M. and Gustafsson, Ö.: Regionally-varying  
 483 combustion sources of the January 2013 severe haze events over eastern China, *Environ. Sci. Technol.*, 49(4),  
 484 2038–2043, doi:10.1021/es503855e, 2015.
- 485 Barnhart, K. R., Anderson, R. S., Overeem, I., Wobus, C., Clow, G. D. and Urban, F. E.: Modeling erosion of  
 486 ice-rich permafrost bluffs along the Alaskan Beaufort Sea coast, *J. Geophys. Res. Earth Surf.*, 119(5), 1155–  
 487 1179, doi:10.1002/2013JF002845, 2014.
- 488 Baskaran, M., Bianchi, T. S. and Filley, T. R.: Inconsistencies between <sup>14</sup>C and short-lived radionuclides-based  
 489 sediment accumulation rates : Effects of long-term remineralization, *J. Environ. Radioact.*, 1–7,  
 490 doi:10.1016/j.jenvrad.2016.07.028, 2016.
- 491 Bauch, H. a., Kassens, H., Naidina, O. D., Kunz-Pirrung, M. and Thiede, J.: Composition and Flux of Holocene  
 492 Sediments on the Eastern Laptev Sea Shelf, Arctic Siberia, *Quat. Res.*, 55(3), 344–351,  
 493 doi:10.1006/qres.2000.2223, 2001a.
- 494 Bauch, H. A., Mueller-Lupp, T., Taldenkova, E., Spielhagen, R. F., Kassens, H., Grootes, P. M., Thiede, J.,  
 495 Heinemeier, J. and Petryashov, V. V.: Chronology of the holocene transgression at the north siberian margin,  
 496 *Glob. Planet. Change*, 31(1–4), 125–139, doi:10.1016/S0921-8181(01)00116-3, 2001b.
- 497 Benner, R. and Opsahl, S.: Early diagenesis of vascular plant tissues : Lignin and cutin decomposition and  
 498 biogeochemical implications, , 59(23), 1995.
- 499 Boudreau, B. P.: Is burial velocity a master parameter for bioturbation?, *Geochim. Cosmochim. Acta*, 58(4),  
 500 1243–1249, doi:10.1016/0016-7037(94)90378-6, 1994.
- 501 Bröder, L., Tesi, T., Salvadó, J. A., Semiletov, I. P. and Dudarev, O. V.: Fate of terrigenous organic matter  
 502 across the Laptev Sea from the mouth of the Lena River to the deep sea of the Arctic interior, , 5003–5019,  
 503 doi:10.5194/bg-13-5003-2016, 2016a.
- 504 Bröder, L., Tesi, T., Andersson, A., Eglinton, T. I., Semiletov, I. P., Dudarev, O. V., Roos, P. and Gustafsson,





- 505 Ö.: Historical records of organic matter supply and degradation status in the East Siberian Sea, *Org. Geochem.*,  
 506 91, 16–30, doi:10.1016/j.orggeochem.2015.10.008, 2016b.
- 507 Bröder, L., Tesi, T., Andersson, A., Semiletov, I. and Gustafsson, Ö.: Bounding cross-shelf transport time and  
 508 degradation in land-ocean carbon transfer. 2017. (submitted)
- 509 Bronk Ramsey, C.: Deposition models for chronological records, *Quat. Sci. Rev.*, 27(1–2), 42–60,  
 510 doi:10.1016/j.quascirev.2007.01.019, 2008.
- 511 Bronk Ramsey, C. and Lee, S.: Recent and Planned Developments of the Program OxCal, *Radiocarbon*, 55(2),  
 512 720–730, doi:10.2458/azu\_js\_rc.55.16215, 2013.
- 513 Canuel, E. A. and Martens, C. S.: Reactivity of recently deposited organic matter : near the sediment-water  
 514 Degradation interface of lipid compounds, *Geochim. Cosmochim. Acta*, 60(10), 1793–1806, 1996.
- 515 Ciais, P., Gasser, T., Paris, J. D., Caldeira, K., Raupach, M. R., Canadell, J. G., Patwardhan, A., Friedlingstein,  
 516 P., Piao, S. L. and Gitz, V.: Attributing the increase in atmospheric CO<sub>2</sub> to emitters and absorbers, *Nat. Clim.*  
 517 *Chang.*, 3(10), 926–930, doi:10.1038/nclimate1942, 2013.
- 518 Conlan, K. E., Lenihan, H. S., Kvitek, R. G. and Oliver, J. S.: Ice scour disturbance to benthic communities in  
 519 the Canadian High Arctic, *Mar. Ecol. Prog. Ser.*, 166, 1–16, doi:10.3354/meps166001, 1998.
- 520 Crichton, K. A., Bouttes, N., Roche, D. M., Chappellaz, J. and Krinner, G.: Permafrost carbon as a missing link  
 521 to explain CO<sub>2</sub> changes during the last deglaciation, , 9(August), doi:10.1038/NGEO2793, 2016.
- 522 Elmquist, M., Zencak, Z. and Gustafsson, Ö.: A 700 year sediment record of black carbon and polycyclic  
 523 aromatic hydrocarbons near the EMEP air monitoring station in Aspövreten, Sweden, *Environ. Sci. Technol.*,  
 524 41(20), 6926–6932, doi:10.1021/es070546m, 2007.
- 525 Farella, N., Lucotte, M., Louchouart, P. and Roulet, M.: Deforestation modifying terrestrial organic transport  
 526 , Brazilian Amazon in the Rio Tapajo, *Org. Geochem.*, 32, 1443–1458, 2001.
- 527 Fry, B. and Sherr, E. B.: δ<sup>13</sup>C Measurements as indicators of carbon flow in marine and freshwater ecosystems,  
 528 *Contrib. Mar. Sci.*, 27, 13–49, 1984.
- 529 Goni, M. A., O'Connor, A. E., Kuzyk, Z. Z., Yunker, M. B., Gobeil, C. and Macdonald, R. W.: Distribution and  
 530 sources of organic matter in surface marine sediments across the North American Arctic margin, *J. Geophys.*  
 531 *Res.*, 118(9), 4017–4035, doi:10.1002/jgrc.20286, 2013.
- 532 Goñi, M. A. and Hedges, J. I.: Sources and reactivities of marine-derived organic matter in coastal sediments as  
 533 determined by alkaline CuO oxidation, *Geochim. Cosmochim. Acta*, 59(14), 2965–2981, doi:10.1016/0016-  
 534 7037(95)00188-3, 1995.
- 535 Goñi, M. A. and Montgomery, S.: Alkaline CuO oxidation with a microwave digestion system: Lignin analyses  
 536 of geochemical samples, *Anal. Chem.*, 72(14), 3116–3121, doi:10.1021/ac991316w, 2000.
- 537 Goñi, M. A., Nelson, B., Blanchette, R. A. and Hedges, J. I.: Fungal degradation of wood lignins: Geochemical  
 538 perspectives from CuO-derived phenolic dimers and monomers, *Geochim. Cosmochim. Acta*, 57(16), 3985–  
 539 4002, doi:10.1016/0016-7037(93)90348-Z, 1993.
- 540 Goñi, M. A., Yunker, M. B., MacDonald, R. W. and Eglinton, T. I.: Distribution and sources of organic  
 541 biomarkers in arctic sediments from the Mackenzie River and Beaufort Shelf, *Mar. Chem.*, 71(1–2), 23–51,  
 542 doi:10.1016/S0304-4203(00)00037-2, 2000.
- 543 Goñi, M. A., O'Connor, A. E., Kuzyk, Z. Z., Yunker, M. B., Gobeil, C. and Macdonald, R. W.: Distribution and  
 544 sources of organic matter in surface marine sediments across the North American Arctic margin, *J. Geophys.*  
 545 *Res. Ocean.*, 118, 4017–4035, doi:10.1002/jgrc.20286, 2013.
- 546 Gordeev, V. V.: Fluvial sediment flux to the Arctic Ocean, *Geomorphology*, 80(1–2), 94–104,



- 547 doi:10.1016/j.geomorph.2005.09.008, 2006.
- 548 Grigoriev, M.: Coastal sediment and organic carbon flux to the Laptev and East Siberian Seas, , 12, 8763, 2010.
- 549 Grigoriev, M. N.: The degradation of coastal permafrost and the organic carbon balance of the Laptev and East  
550 Siberian Seas, , (1987), 2003.
- 551 Günther, F., Overduin, P. P., Yakshina, I. A., Opel, T., Baranskaya, A. V. and Grigoriev, M. N.: Observing  
552 Muostakh disappear: Permafrost thaw subsidence and erosion of a ground-ice-rich Island in response to arctic  
553 summer warming and sea ice reduction, *Cryosphere*, 9(1), 151–178, doi:10.5194/tc-9-151-2015, 2015.
- 554 Hartnett, H., Keil, R., Hedges, J. and Devol, A.: Influence of oxygen exposure time on organic carbon  
555 preservation in continental margin sediments, *Nature*, 391(February), 572–575, doi:10.1038/35351, 1998.
- 556 Hedges, J. I., Blanchette, R. A., Weliky, K. and Devol, A. H.: Effects of fungal degradation on the CuO  
557 oxidation products of lignin: A controlled laboratory study, *Geochim. Cosmochim. Acta*, 52(11), 2717–2726,  
558 doi:10.1016/0016-7037(88)90040-3, 1988.
- 559 Higuchi, T.: Formation and biological degradation of lignins, *Adv Enzym. Relat Areas Mol Biol*, 34, 207–283,  
560 1971.
- 561 Hilton, R. G., Galy, V., Gaillardet, J., Dellinger, M., Bryant, C., O'Regan, M., Gröcke, D. R., Coxall, H.,  
562 Bouchez, J. and Calmels, D.: Erosion of organic carbon in the Arctic as a geological carbon dioxide sink,  
563 *Nature*, 524(7563), 84–87, doi:10.1038/nature14653, 2015.
- 564 Hugelius, G., Strauss, J., Zubrzycki, S., Harden, J. W., Schuur, E. A. G., Ping, C. L., Schirmer, L., Grosse,  
565 G., Michaelson, G. J., Koven, C. D., O'Donnell, J. A., Elberling, B., Mishra, U., Camill, P., Yu, Z., Palmtag, J.  
566 and Kuhry, P.: Estimated stocks of circumpolar permafrost carbon with quantified uncertainty ranges and  
567 identified data gaps, *Biogeosciences*, 11(23), 6573–6593, doi:10.5194/bg-11-6573-2014, 2014.
- 568 IPCC Working Group 1, I., Stocker, T. F., Qin, D., Plattner, G.-K., Tignor, M., Allen, S. K., Boschung, J.,  
569 Nauels, A., Xia, Y., Bex, V. and Midgley, P. M.: IPCC, 2013: Climate Change 2013: The Physical Science  
570 Basis. Contribution of Working Group I to the Fifth Assessment Report of the Intergovernmental Panel on  
571 Climate Change, IPCC, AR5, 1535, 2013.
- 572 Jakobsson, M.: Hypsometry and volume of the Arctic Ocean and its constituent seas, *Geochemistry Geophys.*  
573 *Geosystems*, 3(5), 1–18, 2002.
- 574 Jakobsson, M., Andreassen, K., Bjarnadóttir, L. R., Dove, D., Dowdeswell, J. A., England, J. H., Funder, S.,  
575 Hogan, K., Ingólfsson, Ó., Jennings, A., Krog Larsen, N., Kirchner, N., Landvik, J. Y., Mayer, L., Mikkelsen,  
576 N., Möller, P., Niessen, F., Nilsson, J., O'Regan, M., Polyak, L., Nørgaard-Pedersen, N. and Stein, R.: Arctic  
577 Ocean glacial history, *Quat. Sci. Rev.*, 92, 40–67, doi:10.1016/j.quascirev.2013.07.033, 2014.
- 578 Jones, B. M., Arp, C. D., Jorgenson, M. T., Hinkel, K. M., Schmutz, J. A. and Flint, P. L.: Increase in the rate  
579 and uniformity of coastline erosion in Arctic Alaska, *Geophys. Res. Lett.*, 36(3), 1–5,  
580 doi:10.1029/2008GL036205, 2009.
- 581 Kanevskiy, M., Shur, Y., Strauss, J., Jorgenson, T., Fortier, D., Stephani, E. and Vasiliev, A.: Patterns and rates  
582 of riverbank erosion involving ice-rich permafrost (yedoma) in northern Alaska, *Geomorphology*, 253, 370–  
583 384, doi:10.1016/j.geomorph.2015.10.023, 2016.
- 584 Karlsson, E., Gelting, J., Tesi, T., van Dongen, B., Andersson, A., Semiletov, I., Charkin, A., Dudarev, O. and  
585 Gustafsson, Ö.: Different sources and degradation state of dissolved, particulate, and sedimentary organic matter  
586 along the Eurasian Arctic coastal margin, *Global Biogeochem. Cycles*, (30), 898–919,  
587 doi:doi:10.1002/2015GB005307, 2016.
- 588 Karlsson, E. S., Charkin, A., Dudarev, O., Semiletov, I., Vonk, J. E., Andersson, A., Gustafsson, O. and Arctic,



- 589 I.: Carbon isotopes and lipid biomarker investigation of sources, transport and degradation of terrestrial organic  
 590 matter in the Buor-Khaya Bay, SE Laptev Sea, 1865–1879, doi:10.5194/bg-8-1865-2011, 2011.
- 591 Karlsson, E. S., Brüchert, V., Tesi, T., Charkin, A., Dudarev, O., Semiletov, I. and Gustafsson, Ö.: Contrasting  
 592 regimes for organic matter degradation in the East Siberian Sea and the Laptev Sea assessed through microbial  
 593 incubations and molecular markers, *Mar. Chem.*, 170, 11–22, doi:10.1016/j.marchem.2014.12.005, 2015.
- 594 Keil, R. G., Dickens, A. F., Arnarson, T., Nunn, B. L. and Devol, A. H.: What is the oxygen exposure time of  
 595 laterally transported organic matter along the Washington margin?, *Mar. Chem.*, 92(1–4 SPEC. ISS.), 157–165,  
 596 doi:10.1016/j.marchem.2004.06.024, 2004.
- 597 Kohlbach, D., Graeve, M., A. Lange, B., David, C., Peeken, I. and Flores, H.: The importance of ice algae-  
 598 produced carbon in the central Arctic Ocean ecosystem: Food web relationships revealed by lipid and stable  
 599 isotope analyses, *Limnol. Oceanogr.*, 61(6), 2027–2044, doi:10.1002/lno.10351, 2016.
- 600 Koven, C. D., Ringeval, B., Friedlingstein, P., Ciais, P., Cadule, P. and Khvorostyanov, D.: Permafrost carbon-  
 601 climate feedbacks accelerate global warming, (15), doi:10.1073/pnas.1103910108, 2011.
- 602 Kunst, L. and Samuels, A. L.: Biosynthesis and secretion of plant cuticular wax, *Prog. Lipid Res.*, 42(1), 51–80,  
 603 doi:10.1016/S0163-7827(02)00045-0, 2003.
- 604 Lambeck, K., Rouby, H., Purcell, A., Sun, Y. and Sambridge, M.: Sea level and global ice volumes from the  
 605 Last Glacial Maximum to the Holocene., *Proc. Natl. Acad. Sci. U. S. A.*, 111(43), 15296–303,  
 606 doi:10.1073/pnas.1411762111, 2014.
- 607 Louchouart, P., Lucotte, M. and Farella, N.: Historical and geographical variations of sources and transport of  
 608 terrigenous organic matter within a large-scale coastal environment, *Org. Geochem.*, 30(7), 675–699,  
 609 doi:10.1016/S0146-6380(99)00019-4, 1999.
- 610 McClelland, J. W., Holmes, R. M., Peterson, B. J., Raymond, P. A., Striegl, R. G., Zhulidov, A. V., Zimov, S.  
 611 A., Zimov, N., Tank, S. E., Spencer, R. G. M., Staples, R., Gurtovaya, T. Y. and Griffin, C. G.: Particulate  
 612 organic carbon and nitrogen export from major Arctic rivers, *Global Biogeochem. Cycles*, doi:10.1002/  
 613 2015GB005351, 2016.
- 614 Mueller-Lupp, T., Bauch, H. A., Erlenkeuser, H., Hefter, J., Kassens, H. and Thiede, J.: Changes in the  
 615 deposition of terrestrial organic matter on the Laptev Sea shelf during the Holocene: evidence from stable  
 616 carbon isotopes, *Int. J. Earth Sci.*, 89(3), 563–568, doi:10.1007/s005310000128, 2000.
- 617 Olefeldt, D., Goswami, S., Grosse, G., Hayes, D., Hugelius, G., Kuhry, P., McGuire, A. D., Romanovsky, V. E.,  
 618 Sannel, A. B. K., Schuur, E. A. G. and Turetsky, M. R.: Circumpolar distribution and carbon storage of  
 619 thermokarst landscapes, *Nat. Commun.*, 7, 13043, doi:10.1038/ncomms13043, 2016.
- 620 Parnell, A. C., Phillips, D. L., Bearhop, S., Semmens, B. X., Ward, E. J., Moore, J. W., Jackson, A. L. and Inger,  
 621 R.: Bayesian Stable Isotope Mixing Models, *arXiv Prepr. arXiv ...*, 16, doi:10.1002/env.2221, 2012.
- 622 Pearson, A., McNichol, A. P., Schneider, R. J., Von Reden, K. F. and Zheng, Y.: Microscale AMS 14C  
 623 measurements at NOSAMS, *Radiocarbon*, 40(1), 61–75, 1998.
- 624 Prah, F. G., Ertel, J. R., Goni, M. A., Sparrow, M. A. and Eversmeyer, B.: Terrestrial organic carbon  
 625 contributions to sediments on the Washington margin, *Geochim. Cosmochim. Acta*, 58(14), 3035–3048,  
 626 doi:10.1016/0016-7037(94)90177-5, 1994.
- 627 Romanovskii, N. N., Hubberten, H. W., Gavrilov, A. V., Tumskoy, V. E. and Kholodov, A. L.: Permafrost of the  
 628 east Siberian Arctic shelf and coastal lowlands, in *Quaternary Science Reviews*, vol. 23, pp. 1359–1369., 2004.
- 629 Salvadó, J. A., Tesi, T., Sundbom, M., Karlsson, E., Krusá, M., Semiletov, I. P., Panova, E. and Gustafsson, Ö.:  
 630 Contrasting composition of terrigenous organic matter in the dissolved, particulate and sedimentary organic



- 631 carbon pools on the outer East Siberian Arctic Shelf, *Biogeosciences*, 13(22), 6121–6138, doi:10.5194/bg-13-  
 632 6121-2016, 2016.
- 633 Sánchez-García, L., Alling, V., Pugach, S., Vonk, J., Van Dongen, B., Humborg, C., Dudarev, O., Semiletov, I.  
 634 and Gustafsson, Ö.: Inventories and behavior of particulate organic carbon in the Laptev and East Siberian seas,  
 635 *Global Biogeochem. Cycles*, 25(2), 1–13, doi:10.1029/2010GB003862, 2011.
- 636 Schirrmeister, L., Kunitsky, V., Grosse, G., Wetterich, S., Meyer, H., Schwamborn, G., Babiy, O., Derevyagin,  
 637 A. and Siegert, C.: Sedimentary characteristics and origin of the Late Pleistocene Ice Complex on north-east  
 638 Siberian Arctic coastal lowlands and islands - A review, *Quat. Int.*, 241(1–2), 3–25,  
 639 doi:10.1016/j.quaint.2010.04.004, 2011.
- 640 Schuur, E. A. G., McGuire, A. D., Grosse, G., Harden, J. W., Hayes, D. J., Hugelius, G., Koven, C. D. and  
 641 Kuhry, P.: Climate change and the permafrost carbon feedback, *Nature*, 520(January 2016), 171–179,  
 642 doi:10.1038/nature14338, 2015.
- 643 Semiletov, I., Dudarev, O., Luchin, V., Charkin, A., Shin, K. H. and Tanaka, N.: The East Siberian Sea as a  
 644 transition zone between Pacific-derived waters and Arctic shelf waters, *Geophys. Res. Lett.*, 32(10), 1–5,  
 645 doi:10.1029/2005GL022490, 2005.
- 646 Semiletov, I., Pipko, I., Gustafsson, Ö., Anderson, L. G., Sergienko, V., Pugach, S., Dudarev, O., Charkin, A.,  
 647 Gukov, A., Bröder, L., Andersson, A., Spivak, E. and Shakhova, N.: Acidification of East Siberian Arctic Shelf  
 648 waters through addition of freshwater and terrestrial carbon, *Nat. Geosci.*, 9(April), 361–365,  
 649 doi:10.1038/NEGO2695, 2016.
- 650 Semiletov, I. P.: Aquatic Sources and Sinks of CO<sub>2</sub> and CH<sub>4</sub> in the Polar Regions, *J. Atmos. Sci.*, 56, 1999a.  
 651 Semiletov, I. P.: Destruction of the coastal permafrost ground as an important factor in biogeochemistry of the  
 652 Arctic Shelf waters, *Trans. [Doklady] Russ. Acad. Sci.*, 368(6), 679–682, 1999b.
- 653 Semiletov, I. P., Pipko, I. I., Shakhova, N. E., Dudarev, O. V., Pugach, S. P., Charkin, A. N., Mcroy, C. P.,  
 654 Kosmach, D. and Gustafsson, Ö.: Carbon transport by the Lena River from its headwaters to the Arctic Ocean,  
 655 with emphasis on fluvial input of terrestrial particulate organic carbon vs. carbon transport by coastal erosion,  
 656 *Biogeosciences*, 8(9), 2407–2426, doi:10.5194/bg-8-2407-2011, 2011.
- 657 Semiletov, I. P., Shakhova, N. E., Sergienko, V. I., Pipko, I. I. and Dudarev, O. V.: On carbon transport and fate  
 658 in the East Siberian Arctic land–shelf–atmosphere system, *Environ. Res. Lett.*, 7(1), 15201, doi:10.1088/1748-  
 659 9326/7/1/015201, 2012.
- 660 Semiletov, I. P., Shakhova, N. E., Pipko, I. I., Pugach, S. P., Charkin, A. N., Dudarev, O. V., Kosmach, D. A.  
 661 and Nishino, S.: Space-time dynamics of carbon and environmental parameters related to carbon dioxide  
 662 emissions in the Buor-Khaya Bay and adjacent part of the Laptev Sea, *Biogeosciences*, 10(9), 5977–5996,  
 663 doi:10.5194/bg-10-5977-2013, 2013.
- 664 Shakhova, N., Semiletov, I., Leifer, I., Salyuk, A., Rekant, P. and Kosmach, D.: Geochemical and geophysical  
 665 evidence of methane release over the East Siberian Arctic Shelf, *J. Geophys. Res. Ocean.*, 115(8), 1–14,  
 666 doi:10.1029/2009JC005602, 2010.
- 667 Shakhova, N., Semiletov, I., Leifer, I., Sergienko, V., Salyuk, A., Kosmach, D., Chernykh, D., Stubbs, C.,  
 668 Nicolosky, D., Tumskoy, V. and Gustafsson, Ö.: Ebullition and storm-induced methane release from the East  
 669 Siberian Arctic Shelf, *Nat. Geosci.*, 7(January), 64–70, doi:10.1038/ngeo2007, 2013.
- 670 Shakhova, N., Semiletov, I., Sergienko, V., Lobkovsky, L., Yusupov, V., Salyuk, A., Salomatina, A., Chernykh,  
 671 D., Kosmach, D., Panteleev, G., Nicolosky, D., Samarkin, V., Joye, S., Charkin, A., Dudarev, O., Meluzov, A.  
 672 and Gustafsson, O.: The East Siberian Arctic Shelf: Towards further assessment of permafrost-related methane



- 673 fluxes and role of sea ice, *Philos. Trans. R. Soc. A*, 373(2052), 20140451–, doi:10.1098/rsta.2014.0451, 2015.
- 674 Shakhova, N. E., Sergienko, V. I. and Semiletov, I. P.: The contribution of the East Siberian shelf to the modern  
 675 methane cycle, *Her. Russ. Acad. Sci.*, 79(3), 237–246, doi:10.1134/S101933160903006X, 2009.
- 676 Stein, R. and Macdonald, R. W.: The organic carbon cycle in the Arctic Ocean., 2004.
- 677 Stuiver, M. and Braziunas, T. F.: Modeling Atmospheric <sup>14</sup>C Influences and <sup>14</sup>C Ages of Marine Samples to  
 678 10,000 BC, *Radiocarbon*, 35(1), 137–189, 1993.
- 679 Stuiver, M. and Polach, H. a: *Radiocarbon*, *Radiocarbon*, 19(3), 355–363, doi:10.1021/ac100494m, 1977.
- 680 Tamocai, C., Canadell, J. G., Schuur, E. A. G., Kuhry, P., Mazhitova, G. and Zimov, S.: Soil organic carbon  
 681 pools in the northern circumpolar permafrost region, *Global Biogeochem. Cycles*, 23(2), 1–11,  
 682 doi:10.1029/2008GB003327, 2009.
- 683 Tesi, T., Semiletov, I., Hugelius, G., Dudarev, O., Kuhry, P. and Gustafsson, Ö.: Composition and fate of  
 684 terrigenous organic matter along the Arctic land-ocean continuum in East Siberia: Insights from biomarkers and  
 685 carbon isotopes, *Geochim. Cosmochim. Acta*, 133, 235–256, doi:10.1016/j.gca.2014.02.045, 2014.
- 686 Tesi, T., Muschitiello, F., Smittenberg, R. H., Jakobsson, M., Vonk, J. E., Hill, P., Andersson, A., Kirchner, N.,  
 687 Noormets, R., Dudarev, O., Semiletov, I. and Gustafsson, Ö.: Massive remobilization of permafrost carbon  
 688 during post-glacial warming, *Nat. Commun.*, 7, 13653, doi:10.1038/ncomms13653, 2016a.
- 689 Tesi, T., Semiletov, I. P., Dudarev, O. V., Andersson, A. and Gustafsson, Ö.: Matrix association effects on  
 690 hydrodynamic sorting and degradation of terrestrial organic matter during cross-shelf transport in the Laptev  
 691 and East Siberian shelf seas, *J. Geophys. Res. Biogeosciences*, 121(3), 731–752,  
 692 doi:10.1002/2015JG003067.Received, 2016b.
- 693 Vetrov, A. and Romankevich, E.: *Carbon Cycle in the Russian Arctic Seas*, Springer-Verlag Berlin Heidelberg.,  
 694 2004.
- 695 Vonk, J. E. and Gustafsson, Ö.: Permafrost-carbon complexities, *Nat. Geosci.*, 6(9), 675–676,  
 696 doi:10.1038/ngeo1937, 2013.
- 697 Vonk, J. E., Sánchez-García, L., Semiletov, I., Dudarev, O., Eglinton, T., Andersson, A. and Gustafsson, O.:  
 698 Molecular and radiocarbon constraints on sources and degradation of terrestrial organic carbon along the  
 699 Kolyma paleoriver transect, East Siberian Sea, *Biogeosciences*, 7(10), 3153–3166, doi:10.5194/bg-7-3153-2010,  
 700 2010.
- 701 Vonk, J. E., Sánchez-García, L., van Dongen, B. E., Alling, V., Kosmach, D., Charkin, a., Semiletov, I. P.,  
 702 Dudarev, O. V., Shakhova, N., Roos, P., Eglinton, T. I., Andersson, a. and Gustafsson, Ö.: Activation of old  
 703 carbon by erosion of coastal and subsea permafrost in Arctic Siberia, *Nature*, 489(7414), 137–140,  
 704 doi:10.1038/nature11392, 2012.
- 705 Vonk, J. E., Semiletov, I., Dudarev, O., Eglinton, T. I., Andersson, A., Shakhova, N., Charkin, A., Heim, B. and  
 706 Gustafsson, Ö.: Preferential burial of permafrost-derived organic carbon in Siberian-Arctic shelf waters, *J.*  
 707 *Geophys. Res. Ocean.*, 8410–8421, doi:10.1002/2014JC010261, 2014.
- 708 Winterfeld, M., Goñi, M. A., Just, J., Hefter, J. and Mollenhauer, G.: Characterization of particulate organic  
 709 matter in the Lena River delta and adjacent nearshore zone , NE Siberia – Part 2 : Lignin-derived phenol  
 710 compositions, , 2261–2283, doi:10.5194/bg-12-2261-2015, 2015a.
- 711 Winterfeld, M., Laepple, T. and Mollenhauer, G.: Characterization of particulate organic matter in the Lena  
 712 River delta and adjacent nearshore zone , NE Siberia – Part I : Radiocarbon inventories, , 3769–3788,  
 713 doi:10.5194/bg-12-3769-2015, 2015b.
- 714



715 **Figures and captions**

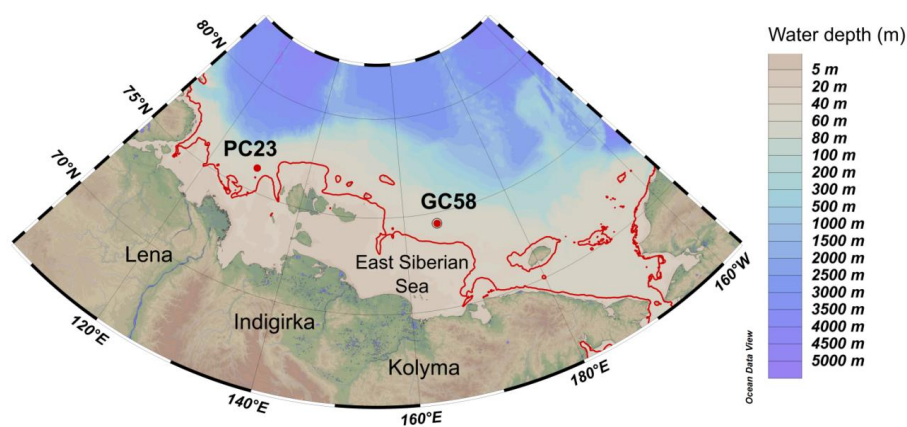
716

717 **Table 1. Radiocarbon ( $^{14}\text{C}$ ) ages of the molluscs retrieved from the sediment core GC58. The  $^{14}\text{C}$  ages are shown in**  
 718 **years BP with an age error (yrs) and as calibrated  $^{14}\text{C}$  ages (cal yrs BP) with one standard deviation ( $\pm 1\sigma$ ) of the**  
 719 **individual  $^{14}\text{C}$  dates. Also shown the  $\delta^{13}\text{C}$  (‰) values of the molluscs.**

Corrected depth* (cm)	NOSAMS Accession nr.	Type	Age $^{14}\text{C}$ (yrs BP)	Age error (yrs)	$\delta^{13}\text{C}$ (‰)	Age $^{14}\text{C}$ (Cal yrs BP)	$1\sigma$
3.5	OS-119395	Mollusc, fragments	895	25	0.55	455	92
8.5	OS-120688	Mollusc, fragments	>Modern	-	1.70	45	32
34.5	OS-120689	Mollusc, fragments	2,260	20	1.55	1,806	125
39.5	OS-120690	Mollusc, fragments	2,210	15	1.55	1,746	122
47.5	OS-123161	Mollusc, fragments	7,960	35	0.90	8,372	110
51.5	OS-119396	Mollusc, fragments	8,010	25	1.06	8,429	112
54.5	OS-120691	Mollusc, fragments	8,020	20	0.49	8,441	113
65.5	OS-119397	Mollusc, <i>Macoma calcaea</i>	8,780	25	-2.46	9,372	117
72.5	OS-120692	Mollusc, fragments	8,880	20	-0.91	9,499	122
78.5	OS-120693	Mollusc, fragments	8,950	25	-0.79	9,595	132

720 \*Corrected depth is the original depth + 3 cm to account for core top loss during sampling (Sect 2.4).

721



722

723

Figure 1. Map of the Eastern Siberian Arctic Shelf showing the location of the sampling site (Station SWERUS C3-1-58) (Schlitzer, R., Ocean Data View, <http://odv.awi.de>, 2015). Also shown in the map is the location of the sediment core PC23 (Station SWERUS C3-1-23, Tesi et al., 2016a). The red line marks the isobath (34 m water depth) which is approximately where the coast line was in the beginning of the sediment archive (GC58) ~9,500 cal yrs BP (Lambeck et al., 2014).

725

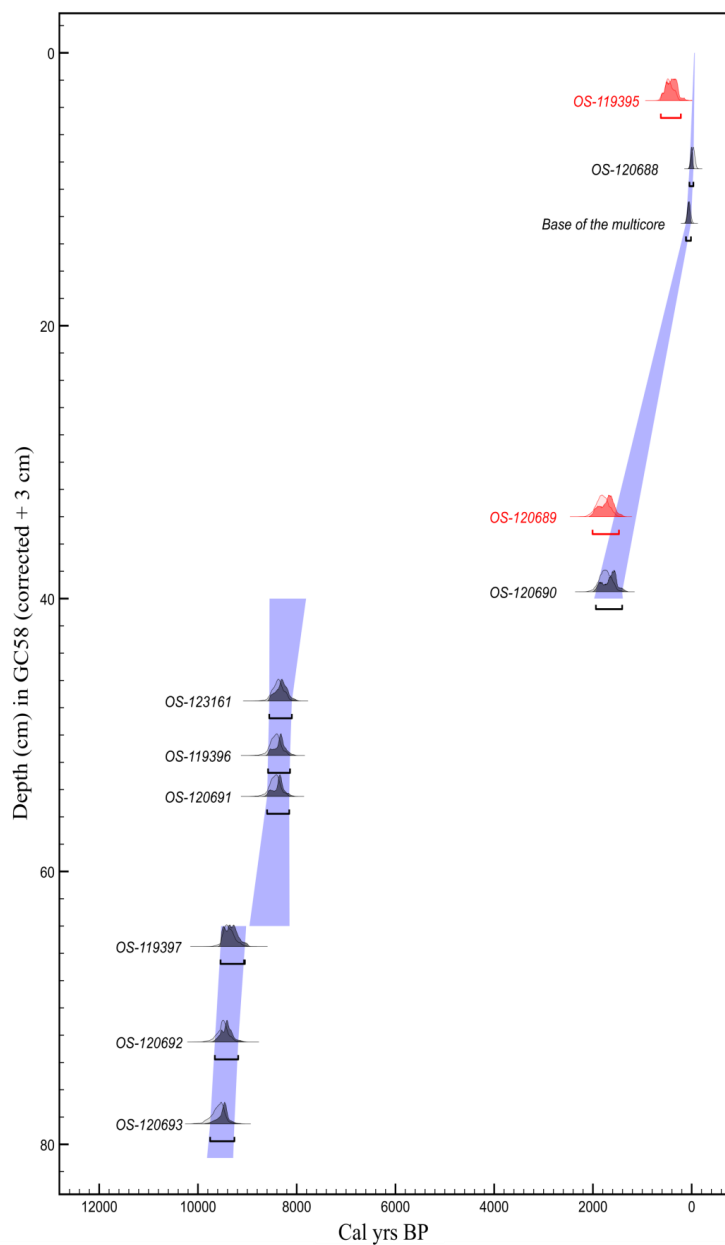
726

727

728



729



730

731

732

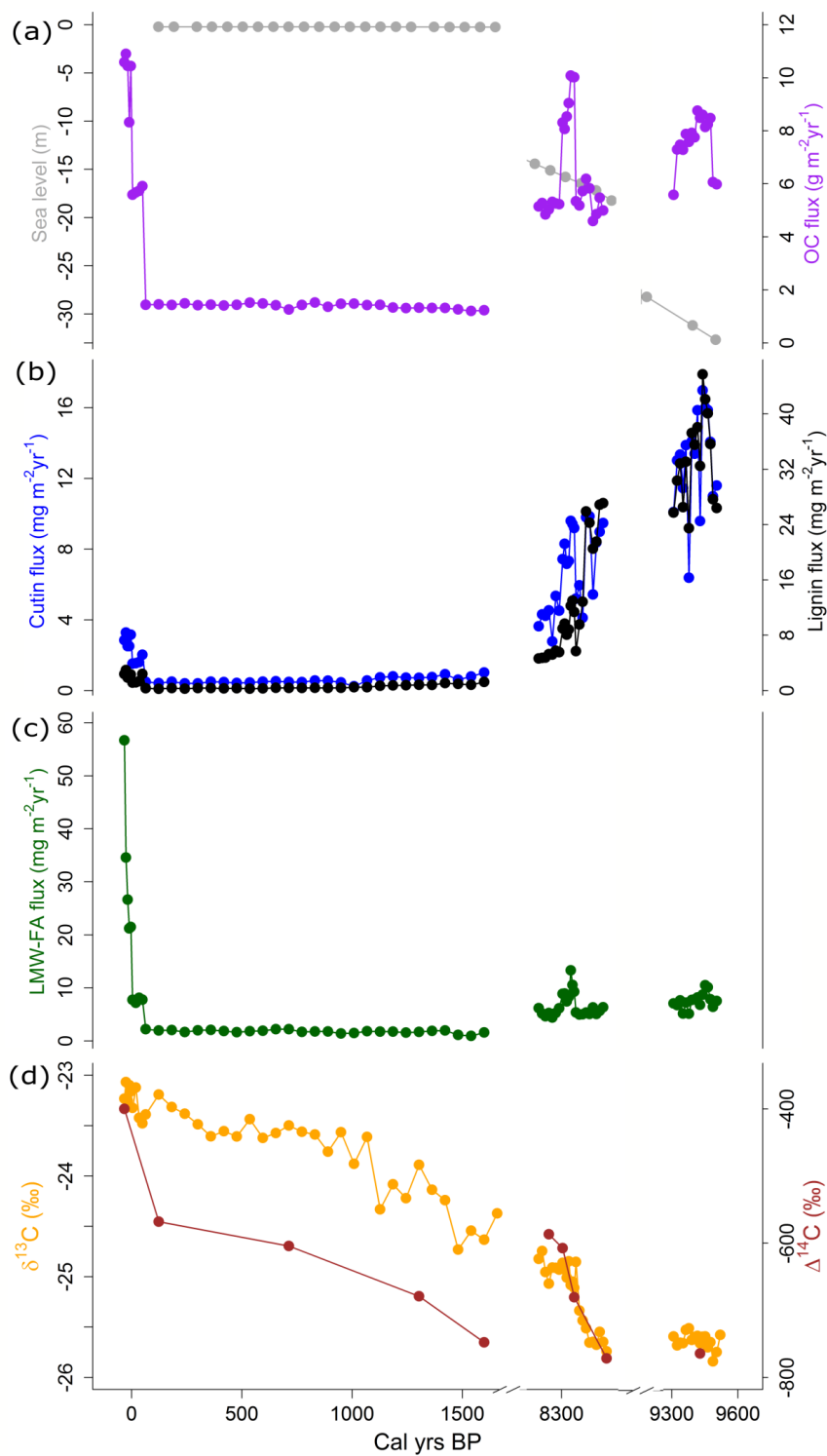
733

734

735

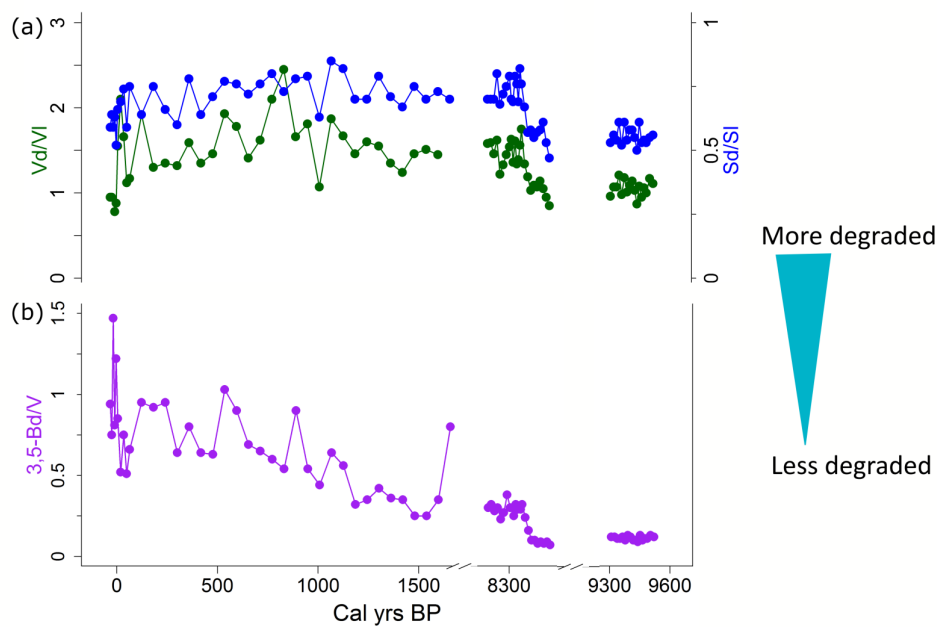
Figure 2. An age-depth model of the sediment core GC58 based on radiocarbon ( $^{14}\text{C}$ ) dated molluscs (see Table 1) and  $^{210}\text{Pb}$  (base of a multicore collected at the same location). All the modelled dates were calibrated with Marine13 calibration curve. A  $\Delta R$  value of  $50 \pm 100$  yrs was used to account for the differences in the local reservoir age. The core GC58 dates back  $\sim 9,500$  cal yrs BP.







737 **Figure 3. Organic matter composition of the sediment core GC58. The x-axis has breaks due to gaps in the sediment**  
738 **chronology. (a) Organic carbon fluxes ( $\text{g m}^{-2} \text{yr}^{-1}$ ) were high at the bottom of the core. The high fluxes at the top of**  
739 **the core are likely related to the merging of two dating system ( $^{210}\text{Pb}$  and  $^{14}\text{C}$ , see Sect. 3.2). The sea level rose rapidly**  
740 **in the early Holocene (Lambert et al., 2014). (b) Both lignin and cutin fluxes ( $\text{mg m}^{-2} \text{yr}^{-1}$ ) decrease toward the core**  
741 **top. High fluxes at the top of the core are influenced by the OC fluxes and likely do not show an actual increase in the**  
742 **fluxes of lignin and cutin (see Sect. 3.2). (c) Low molecular weight fatty acids (LMW-FA) show an influence of marine**  
743 **organic matter at the top of the core. (d) The  $\delta^{13}\text{C}$  (‰) values illustrate a gradual shift from terrestrial dominated to**  
744 **more marine dominated input of organic matter towards the core top. The  $\Delta^{14}\text{C}$  (‰) values (corrected for the time**  
745 **between the deposition and the measurement) show that the bulk organic carbon is older at the bottom of the core**  
746 **than at the core top. The drop in the  $\Delta^{14}\text{C}$  values  $\sim 1,700$  cal yrs BP is likely an artefact caused by the age model used**  
747 **to correct for the  $\Delta^{14}\text{C}$  values.**  
748



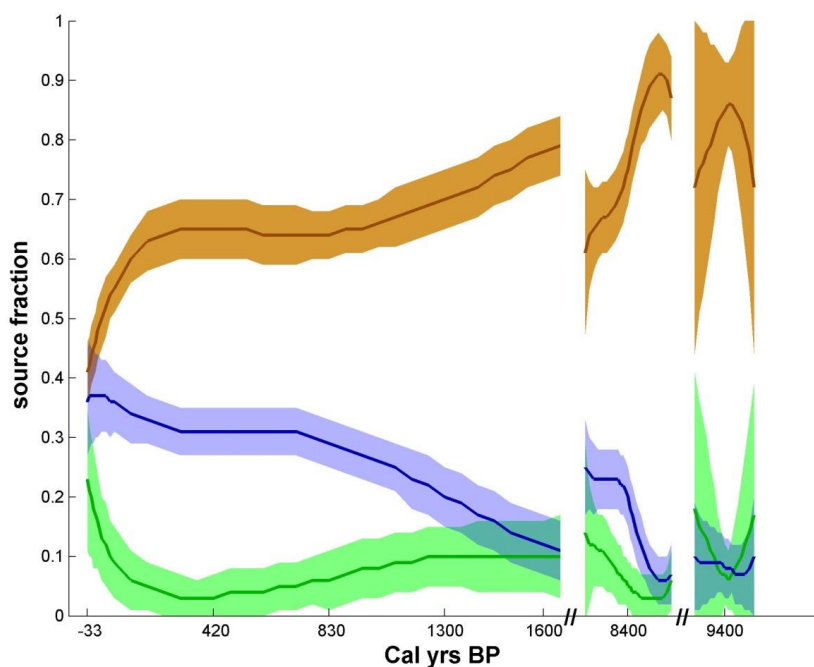
749

750

**Figure 4.** Degradation proxies for terrestrial organic carbon in the sediment core GC58. The x-axis has breaks due to gaps in the sediment chronology. (a) Syringyl acid to syringaldehyde (Sd/SI) and vanillic acid to vanillin (Vd/Vl) ratios are a lignin-phenol based degradation proxy. (b) Also the ratio of 3,5-dihydrobenzoic acid to vanillyl phenols (3,5-Bd/V) provides information on degradation of terrestrial organic carbon. Higher values imply more degraded material for all the ratios as illustrated with the turquoise arrow. The 3,5-Bd/V values suggest a gradual increase in degradation from the bottom of the core to the top.

755

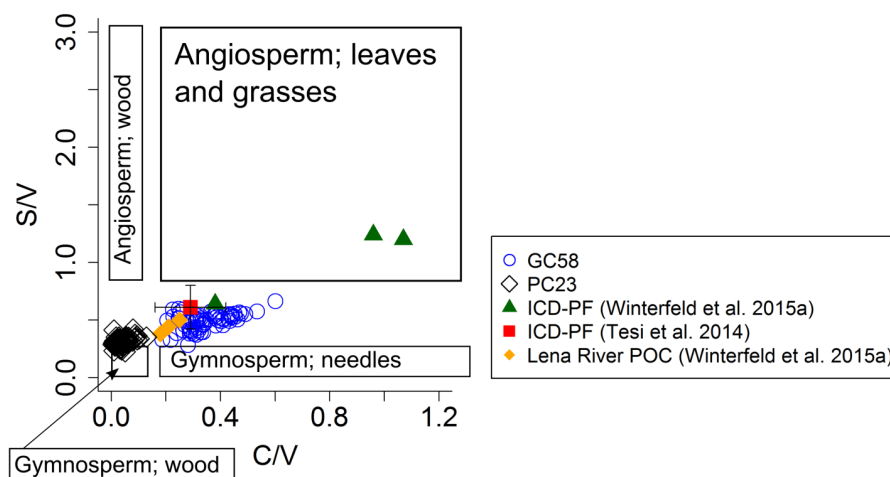
756



757

758 **Figure 5. Dual-carbon isotope ( $\delta^{13}\text{C}$ ,  $\Delta^{14}\text{C}$ ) based source apportionment of organic carbon (OC) illustrates fractions**  
759 **(%; mean  $\pm$  SD) of old Pleistocene permafrost (ICD-PF) in brown, thaw of active-layer permafrost (topsoil-PF) in**  
760 **green and primary production (marine OC) in blue of the sediment core GC58. The ICD-PF is the dominant fraction**  
761 **throughout the core.**

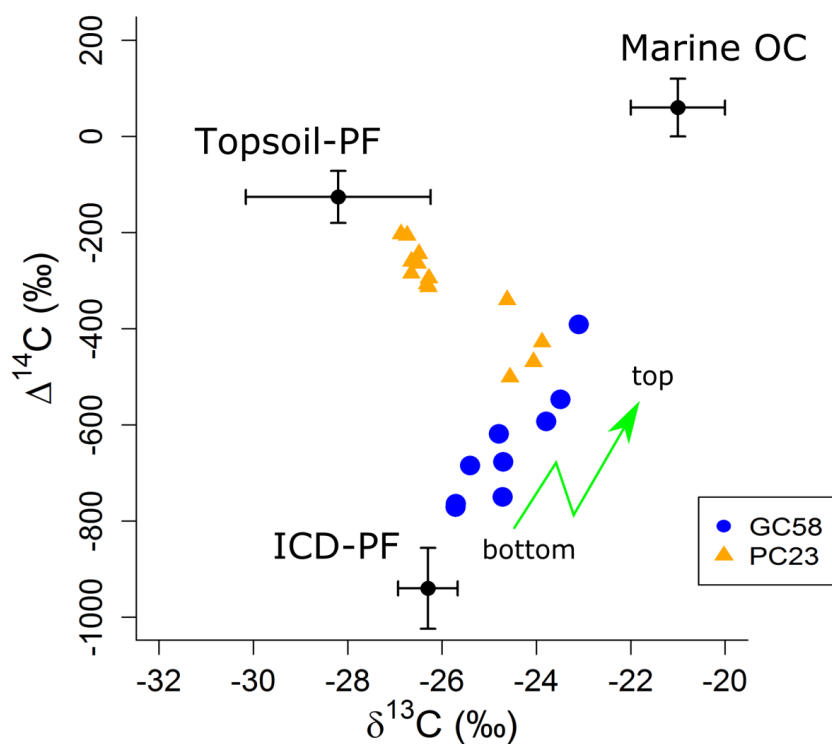
762



763

764 **Figure 6.** Lignin composition of the sediment core GC58 (black circles). The ratio between cinnamyl and vanillyl  
765 phenols (C/V) is used as a proxy to distinguish between soft and woody plant tissues. The ratio of syringyl to vanillyl  
766 phenols (S/V) indicates the difference between gymnosperm and angiosperm plants. The boxes indicate typical values  
767 for S/V and C/V ratios characterising different plant material (ranges from Goñi and Montgomery, 2000). Measured  
768 S/V and C/V ratios for Ice Complex Deposit permafrost (ICD-PF) are shown with green triangles (Winterfeld et al.,  
769 2015a) and with an orange square ( $\pm$ standard deviation) (Tesi et al., 2014). Measured S/V and C/V ratios for topsoil-  
770 PF (Lena River POC) are illustrated with orange diamonds (Winterfeld et al., 2015a). Also shown the lignin  
771 composition of the sediment core PC23 (blue diamonds) from the Laptev Sea.

772



773

774 Figure 7. Dual-carbon isotope ( $\delta^{13}\text{C}$ ,  $\Delta^{14}\text{C}$ ) composition of the sediment cores GC58 and PC23. Topsoil-PF refers to  
775 organic matter from the active-layer of permafrost, ICD-PF to relict Pleistocene Ice Complex Deposit permafrost  
776 (Yedoma) and marine OC to organic matter from primary production. The end-member values for different sources  
777 are taken from the literature (Bröder et al., 2016b; Tesi et al., 2016a). The green arrow points to the direction from  
778 the bottom to the top of the core (GC58).